Correspondence to:
D. V. Kent,
dvk@ldeo.columbia.edu

Magnetochronology of the Entire Chinle Formation (Norian Age) in a Scientific Drill Core From Petrified Forest National Park (Arizona, USA) and Implications for Regional and Global Correlations in the Late Triassic

Dennis V. Kent[1,2] **, Paul E. Olsen**[2] **, Christopher Lepre**[1,2] **, Cornelia Rasmussen**[3,4] **, Roland Mundil**[5] **, George E. Gehrels**[6] **, Dominique Giesler**[6] **, Randall B. Irmis**[3,7] **, John W. Geissman**[8] **, and William G. Parker**[9]

[1]Department of Earth and Planetary Sciences, Rutgers University, Piscataway, NJ, USA, [2]Lamont-Doherty Earth Observatory, Columbia University, Palisades, NY, USA, [3]Department of Geology and Geophysics, University of Utah, Salt Lake City, UT, USA, [4]Institute for Geophysics, Jackson School of Geosciences, University of Texas at Austin, Austin, TX, USA, [5]Berkeley Geochronology Center, Berkeley, CA, USA, [6]Department of Geosciences, University of Arizona, Tucson, AZ, USA, [7]Natural History Museum of Utah, University of Utah, Salt Lake City, UT, USA, [8]Department of Geosciences, University of Texas at Dallas, Richardson, TX, USA, [9]Petrified Forest National Park, Petrified Forest, AZ, USA

Abstract Building on an earlier study that confirmed the stability of the 405-kyr eccentricity climate cycle and the timing of the Newark-Hartford astrochronostratigraphic polarity time scale back to 215 Ma, we extend the magnetochronology of the Late Triassic Chinle Formation to its basal unconformity in scientific drill core PFNP-1A from Petrified Forest National Park (Arizona, USA). The 335-m-thick Chinle section is imprinted with paleomagnetic polarity zones PF1r to PF10n, which we correlate to chrons E17r to E9n (~209 to 224 Ma) of the Newark-Hartford astrochronostratigraphic polarity time scale. A sediment accumulation rate of ~34 m/Myr can be extended down to ~270 m, close to the base of the Sonsela Member and the base of magnetozone PF5n, which we correlate to chron E14n that onsets at 216.16 Ma. Magnetozones PF5r to PF10n in the underlying 65-m-thick section of the mudstone-dominated Blue Mesa and Mesa Redondo members plausibly correlate to chrons E13r to E9n, indicating a sediment accumulation rate of only ~10 m/Myr. Published high-precision U-Pb detrital zircon dates from the lower Chinle tend to be several million years older than the magnetochronological age model. The source of this discrepancy is unclear but may be due to sporadic introduction of juvenile zircons that get recycled. The new magnetochronological constraint on the base of the Sonsela Member brings the apparent timing of the included Adamanian-Revueltian land vertebrate faunal zone boundary and the Zone II to Zone III palynofloral transition closer to the temporal range of the ~215 Ma Manicouagan impact structure in Canada.

1. Introduction

A major goal of the first phase of the Colorado Plateau Coring Project (Olsen et al., 2018) was to obtain a reference section of Late Triassic sedimentation on the Colorado Plateau, which was accomplished by recovering an approximately 335-m-thick stratigraphic section of the largely fluvial Chinle Formation in scientific drill core PFNP-1A from Petrified Forest National Park (PFNP), northeastern Arizona, USA (35.09°N 250.20°E; Figure 1). This core allows us, for the first time, to study the entire Chinle Formation in unquestionable superposition to facilitate correlation with key Triassic sections and events, which previously had been challenging due to lateral facies changes on the local and regional scale (Martz & Parker, 2010). A prime objective was to obtain a diagnostic magnetostratigraphic polarity sequence directly supported by high-precision U-Pb detrital zircon dates that could be used to correlate to and thereby test the validity of the Newark-Hartford astrochronostratigraphic polarity time scale (N-H APTS; Kent et al., 2017, and references therein). A positive test was obtained from combined paleomagnetic (magnetozones PF1r to PF5n) and geochronologic (CA-TIMS detrital zircon ages from five stratigraphic levels) studies of the upper ~240 m stratigraphic depth (msd) in core PFNP-1A of the Chinle Formation (lower Owl Rock Member, the Petrified Forest Member including the distinctive Black Forest Bed, and the upper Sonsela Member). The integrated chronology provided dates
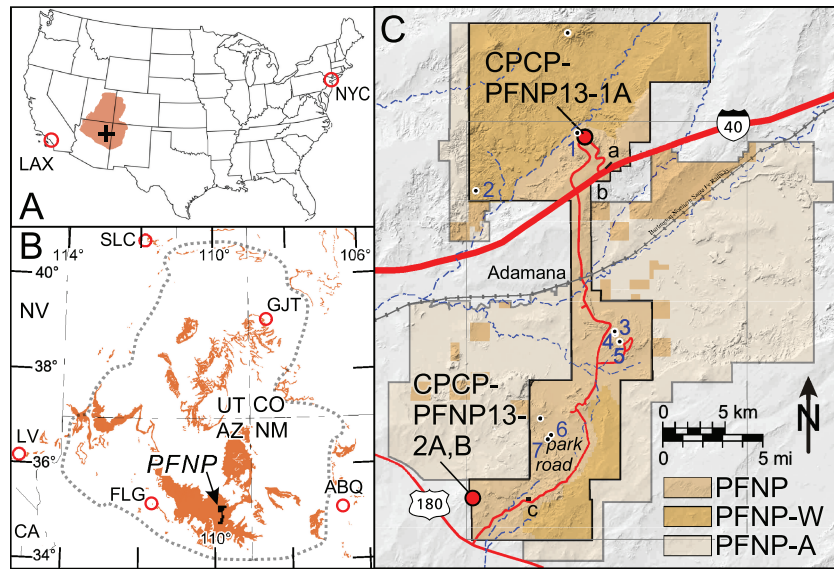
Figure 1. Location map of (a) Colorado Plateau in conterminous United States, (b) sketch map showing outline of Colorado Plateau and outcrops of Triassic strata, and (c) sketch map of Petrified Forest National Park showing locations of scientific drill core CPCP13-1A (referred to here as PFNP-1A). Locations of outcrop samples for high-precision U-Pb detrital zircon dating (see Table S4 for references and dates) are indicated by small circles with numbers, keyed as follows: 1: BFB; 2: KWI; 3: SS-7; 4: TPs; 5: SBJ; 6: GPL; 7: GPU (Ramezani et al., 2011). Geographic coordinates were not available for sample P57-C. Samples SS-28 and SS-24 are from Hunt Valley, ~25 km southest of PFNP. Abbreviations: (a) NYC, New York City; LAX, Los Angeles. (b) UT, Utah; CO, Colorado; NM, New Mexico; AZ, Arizona; NV, Nevada; CA, California; LV, Los Vegas; SLC, Salt lake City; GJT, Grand Junction; FLG, Flagstaff; ABQ, Albuquerque. (c) PFNP, Petrified Forest National Park.

indistinguishable from ages predicted by the N-H APTS using the magnetostratigraphic correlations back to 215 Ma, strongly supporting the 405-kyr Milankovitch climate cycle used to pace the N-H APTS as an accurate time keeper in the geologic record (Kent et al., 2018; see also Commentary by Hinnov, 2018).

The high-precision U-Pb detrital zircon ages from samples of the Petrified Forest and upper Sonsela members in core PFNP-1A reported in Kent et al. (2018) provided a chronostratigraphy that was in excellent overall agreement with the high-precision U-Pb zircon geochronology of samples (BFB, KWI and GPU) from outcrops of the same Petrified Forest and upper Sonsela members previously reported by Ramezani et al. (2011): both sets of U-Pb ages supported a regular sediment accumulation rate of ~34 m/Myr as delineated by the magnetochronology over this stratigraphic interval. However, U-Pb dates obtained by Ramezani et al. (2011) from lower in the Chinle Formation pointed to a marked change in the sedimentation regime including possible hiatuses within the Sonsela Member. For example, their sample GPL from a sand/siltstone bed in the middle of the Sonsela Member yields an U-Pb age that is several million years older than the age expected from a linear extrapolation of the age-depth trends in the immediately overlying parts of the Sonsela and Petrified Forest members. The possibility of an unconformity within the Sonsela Member has direct implications for the age and pacing of the major Adamanian-Revueltian land vertebrate faunal zone boundary that occurs within the Sonsela Member (see Martz & Parker, 2017, for discussion of updated concepts and terminology).

In anticipation that the rather anomalous U-Pb detrital zircon ages of outcrop samples of the lower Chinle Formation (Ramezani et al., 2011) will be better constrained by U-Pb detrital zircon analyses of lithostratigraphically correlative portions of core PFNP-1A that are in progress, we extend magnetostratigraphic sampling and analysis for the rest of the Chinle Formation recovered in core PFNP-1A, from where we stopped (Kent et al., 2018) at ~240 msd in the mid-Sonsela down through the rest of the Sonsela Member and the entire Blue Mesa Member and the Mesa Redondo Member, to the unconformable contact with the Moenkopi Formation at ~355 msd. The new results allow us to offer a testable age model for the entire Chinle Formation based on a straightforward correlation of the magnetostratigraphy to the N-H APTS. The new age model shows that the Blue Mesa and Mesa Redondo members had a substantially lower sediment accumulation rate than
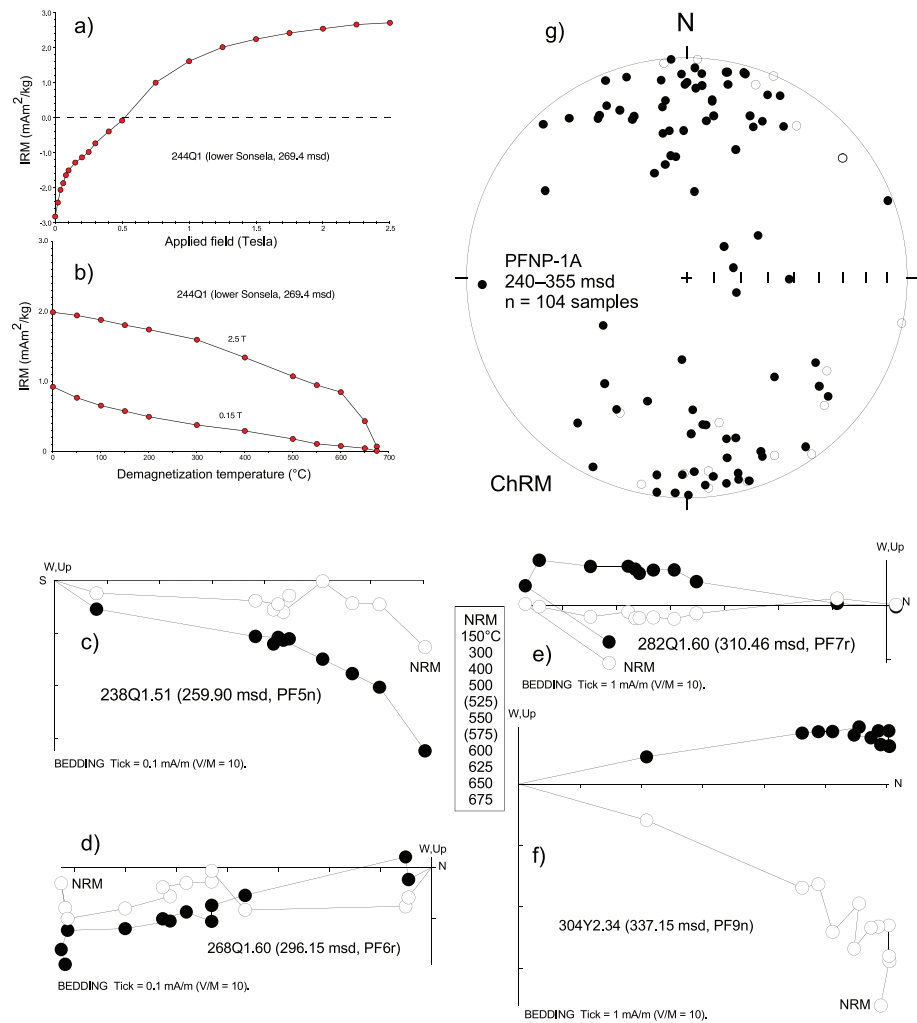
Figure 2. Representative paleomagnetic data for lower Chinle Formation in core PFNP-1A. (a) isothermal remanent magnetization acquisition for a sample from the lower Sonsela Member. (b) Thermal demagnetization of two orthogonal components of isothermal remanent magnetization, one induced in 2.5 T and the other at 0.15 T, as labeled. (c–f) Orthogonal vector end-point plots of progressive thermal demagnetization of natural remanent magnetization (NRM) of four samples. (g) Equal area projection of accepted characteristic remanent magnetization directions of samples from the lower Chinle Formation in core PFNP-1A.

the overlying Sonsela and Petrified Forest members but it does not require a significant hiatus within the Sonsela Member. If the magnetochronology is correct, the resulting large and variable age discrepancies of the U-Pb detrital zircon ages reported by Ramezani et al. (2011) for the lower Chinle Formation implies pervasive recycling of zircons with little detected addition of juvenile air fall zircons in this part of the section, at least as represented in the sandstone samples that have been published thus far.

2. Analytical Approach

The geologic context and logistics of the coring are described in detail elsewhere (Olsen et al., 2018). The paleomagnetic sampling, laboratory measurement and analytical procedures were essentially the same as described for the previous study (Kent et al., 2018). In the present case, a suite of oriented subsamples were extracted from ~280 to 410 m core depth (mcd; ~240–355 msd) from the finest-grained, red, and/or purple-colored sediment facies available in each core section, wherever possible. The subsamples tended to be friable and were carefully trimmed with a bandsaw to 5–10 cc cubes for measurement of their znatural remanent magnetizations (NRMs). Progressive thermal demagnetization in nominally a dozen temperature

steps was used to isolate the stable magnetization component of the NRM most likely to be early acquired, which was carried predominantly by hematite (Figures 2a and 2b). A least-squares linear fit using principal-component analysis over the three to seven (typically five) demagnetization steps in the range of 300–600°C and anchored to the origin (Figures 2c–2f) was used to assess the characteristic remanent magnetization (ChRM) in each sample. Results were deemed acceptable if the maximum angular deviation (MAD; Kirschvink, 1980) was no larger than 16°; 27 samples were rejected based on these criteria, plus 7 samples with inclinations greater than 60° that suggest residual overprinting, and 8 samples in an interval that was adversely affected by a change in the drill bit. A total of 104 of the 142 samples analyzed (74%) were deemed to have valid ChRM data, about the same as the success rate in our study of the upper Chinle in this drill core (Table S1 in the supporting information). This provided a nominal resolution of about 1 sample with acceptable ChRM data per msd over the sampled 115-m stratigraphic interval although other criteria mostly related to validating core orientation by inspection of core photographs were also used to interpret the paleomagnetic data.

Taking into account the 30° deviation from vertical of the drill core (to facilitate orientation of the cores in the flat-lying beds especially in the absence of any persistent overprints) at an azimuth of 135° (to avoid a Bidahochi lava feeder dike), the ChRM directions are noisy but tend to fall into two populations (Figure S1g in the supporting information): a shallow north-directed group interpreted to represent normal polarity and a shallow south-directed group reflecting reverse polarity of the Late Triassic geomagnetic field. The mean ChRM direction (inverting southerly directions to common normal polarity) is declination, D=356.6°, inclination, I=6.0°, radius of circle of 95% confidence, a95=7° for n=104 samples. The expected directions for the Chinle Formation at the core site locality can be bracketed by the 230 and 210 Ma reference poles for North America (Kent & Irving, 2010), which give D=343.2°, I=13.5° for 230 Ma, and D=350.9°, I=20.6° for 210 Ma, corresponding to similar paleolatitudes of 6.8°N±5.7° and 10.7°N±2.9°, respectively. The shallower than expected mean ChRM directions observed for the Chinle in core PFNP-1A (Kent et al., 2018; *this study*) as well as in outcrop (Steiner & Lucas, 2000) can be attributed to sedimentary inclination flattening that is typical of many Triassic continental (nonmarine) red beds with early-acquired detrital remanent magnetizations (Kent & Tauxe, 2005).

The ChRM direction for each sample was converted to a virtual geomagnetic pole (VGP) whose latitude with respect to the 210 Ma reference (north) pole (the same as for the upper Chinle results) and referred to as rVGP latitude is used to interpret polarity (toward +90° for normal, −90° for reverse polarity). A plot of rVGP latitudes with depth in core PFNP-1A (Figure 2) shows a series of magnetic polarity zones based on two or more consecutive samples with the same polarity. These magnetozones are designated from stratigraphically higher to lower and continuing from the upper Chinle magnetostratigraphy reported earlier as PF5n, PF5r, etc., to normal polarity magnetozone PF10n whose base is the unconformable contact of the Mesa Redondo Member of the Chinle Formation with the underlying Holbrook Member of the Moenkopi Formation. An interval between about 352–357 mcd had a lot of rubble and disturbed sediment core, which we ascribe to effects of a change in drill bit (from Q to Y); we do not interpret the scattered magnetization directions from this interval.

What we regard as the simplest correlation of the magnetic polarity stratigraphy to the N-H APTS is shown in Figure 3 and tabulated in Table S2. Magnetozone PF5n is the downward extension of the lowermost normal polarity magnetozone found in the earlier study (Kent et al., 2018) and most probably correlates to chron E14n whose onset is at 216.16 Ma. This correlation would be consistent with the sediment accumulation rate of around 34 m/Myr that was calculated for the upper part of the Chinle Formation. In contrast, the sequence of ten magnetozones (PF5r to PF10n) in the Blue Mesa and Mesa Redondo members forms a busier pattern plausibly correlating to chrons E13r to E9n that would indicate a much lower sediment accumulation rate of only about 10 m/Myr. In this case, the unconformable base of the Chinle Formation is projected to occur within chron E9n at ~224 Ma. Other correlations are of course possible. For example, PF9n and PF10n may correspond to E11n and E10n, respectively, with the very thin PF8n representing a localized remagnetization; this would put the local base of the Mesa Redondo Member at about 222.5 Ma. In the Sonsela Member, PF5n could be a concatenation of parts of E14n and E13n. While not precluded by the available age constraints, such alternative schemes would require more complicated age-depth relationships than the one shown for the preferred and more testable correlation scheme.
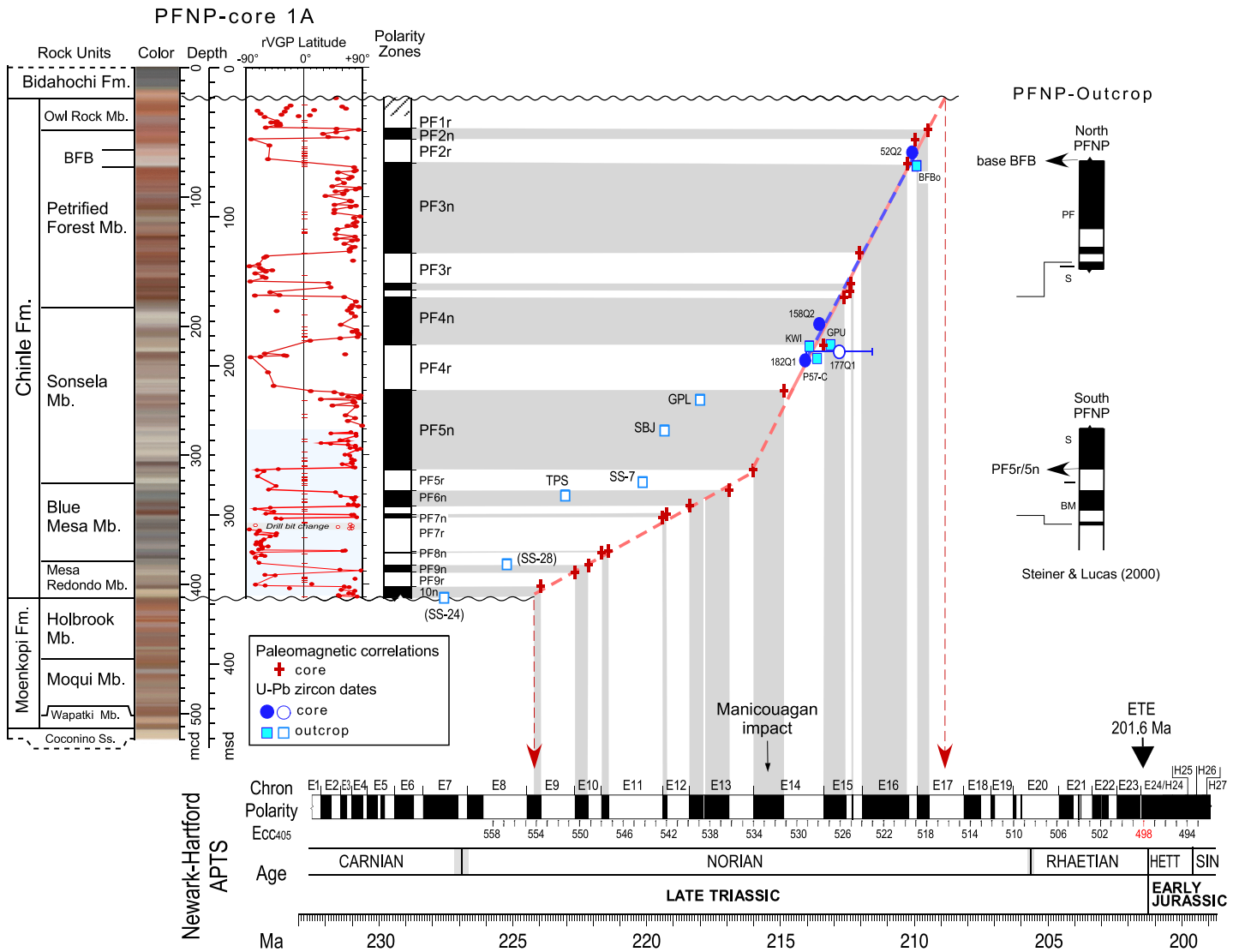
Figure 3. Chronostratigraphic correlations of Chinle Formation in core PFNP-1A (Olsen et al., 2018) to Newark-Hartford APTS (Kent et al., 2017). Column labeled rVGP latitude shows sample ChRM directions converted to virtual geomagnetic poles whose rotated latitudes with respect to the mean 210 Ma reference pole for North America (Kent & Irving, 2010) are plotted versus core (mcd) and stratigraphic (msd) depth in core PFNP-1A. Positive (northerly) and negative (southerly) rVGP latitudes correspond to normal and reverse polarity, delineated in polarity column by white and black bars, respectively; ticks on zero axis are rejected samples. Paleomagnetic data down to 280 mcd (PF1r to PF5n) are from Kent et al. (2018), data from 280 to 410 mcd (PF5n to PF10n) are reported here. High-precision U-Pb zircon dates from core PFNP-1A are from Kent et al. (2018) (filled circles accepted dates used in age model, open circles not used in age model) and from outcrop from Ramezani et al. (2011) using lithostratigraphic section of Atchley et al. (2013); Figure 4) for correlation to core PFNP-1A (filled squares accepted dates included in age model, open squares not used in age model including SS-28 and SS-24 (in parentheses) from Hunt Valley ~25 km southeast of PFNP with less certain lithostratigraphic registry to PFNP-1A). Age model for upper Chinle Formation (Owl Rock, Petrified Forest, and mid-Sonsela members) is based on integrated U-Pb dates and magnetic polarity stratigraphy correlated to Newark-Hartford APTS is shown by dashed blue and solid red linear regression lines from Kent et al. (2018). Age model for lower Chinle Formation (lower Sonsela, Blue Mesa and Mesa Redondo members) is based on magnetic polarity stratigraphy correlated to Newark-Hartford APTS is shown by dashed red line segments. Shown for reference are the timing of the Manicouagan impact crater (Ramezani et al., 2005) and of the ETE (end-Triassic extinction event), which was used as anchor point for N-H APTS, where Ecc405 are 405-kyr peak eccentricities counted back from the most recent peak (Kent et al., 2017). Magnetic polarity stratigraphy by Steiner and Lucas (2000) for what seemed to be a long sequential outcrop section of the Chinle Formation actually contains a stratigraphic gap of ~100 m between the sections sampled in the north and south PFNP (see text for discussion), which are shown here at the same stratigraphic thickness scale (msd) as core PFNP-1A with suggested levels of correlations by arrows and lines. BFB, Black Forest Bed, PF, Petrified Forest Member, S, Sonsela Member, BM, Blue Mesa Member. Note that single sample-level polarity intervals have been removed from the south PFNP section for clarity whereas the lowermost normal polarity interval has been promoted from tentative because it appears to be defined by two stratigraphically consecutive samples with normal polarity in Fig. 8 of Steiner and Lucas (2000). Additional details and explanations are in Figure S1, which includes a problematic composite magnetostratigraphic section from southern PFNP by Zeigler et al. (2017).

3. Consistency of the Preferred Magnetochronology

There have been several magnetostratigraphic studies of exposures of the Chinle Formation in Petrified Forest National Park. The classic study by Steiner and Lucas (2000) sampled a 150-m-thick composite section, the upper part in northern PFNP from the Petrified Forest Member from just below the distinctive Black Forest Bed near Chinde Point (where core PFNP-1A was recovered) and the lower part in southern PFNP at Blue Mesa. Although the reported thickness is about 25% less, the magnetostratigraphic sequence of the upper ~75-m-thick section correlates well to the ~100-m-thick interval from the top of PF3n (base of the Black Forest Bed) to the upper part of PF4n (base of the Petrified Forest Member) in PFNP-1A (Figure 3). Steiner and Lucas (2000) used what they regarded as the base of the Sonsela Member as the correlative datum to tie the two sections together as described in greater detail by Heckert and Lucas (2002). However, subsequent bed-by-bed lithostratigraphic mapping and correlation has shown that about 100 m of section was missed by this correlation (Martz & Parker, 2010). What Steiner and Lucas (2000) regarded as Sonsela Member in the northern section is only a small part of a much thicker unit. Based on Martz and Parker (2010), this missing section was shown explicitly in a diagram and discussed by Olsen et al. (2011), with further endorsement of the sampling gap provided by Zeigler et al. (2017). This miscorrelation illustrates the kind of uncertainties attendant to long-distance correlation of fluvial units based largely on relatively vague lithostratigraphic criteria (Ramezani et al., 2011) and one of the rationales for obtaining unambiguous superposition for the Chinle Formation through scientific drilling. Nonetheless, taking this sampling gap into account shows that the lower part of the composite (from Blue Mesa) of Steiner and Lucas (2000) correlates to PF5n in the lower Sonsela Member down into PF7r within the Blue Mesa Member in core PFNP-1A (Figure 3). Note that Olsen et al. (2011), lacking the core data, correlated the upper and lower sections of the Steiner and Lucas (2000) composite one N-H APTS magnetochron younger than here. In any case, the intervening gap in the composite section is not an unconformity because that interval is present in core PFNP-1A; the gap is simply an artifact of lithostratigraphic miscorrelation.

Zeigler et al. (2017) sampled the Blue Mesa and lower Sonsela members in what appears to be virtually the same locality in southern PFNP (Blue Mesa section; Figure S1) that constituted the lower section of Steiner and Lucas (2000). Although only sampled at ~3 m intervals, Zeigler et al. (2017) suggested that their magnetic polarity sequence for the Blue Mesa and lower Sonsela members in the Blue Mesa section (and stratigraphically subtiguous Tepee section) compared favorably to that found by Steiner and Lucas (2000). The magnetic stratigraphy of the overlying interval of the Sonsela Member sampled in The Peninsula section was an effort to fill in the recognized sampling gap in the Steiner and Lucas (2000) study that in the Blue Mesa area terminated upward at the base of the Sonsela Member, which was explicitly not sampled because of the coarse grain size of the unit there. Indeed, the magnetic record obtained by Zeigler et al. (2017) for The Peninsula section of the Sonsela Member did not yield a recognizable polarity sequence for correlation, perhaps because as the authors suggested the coarse grain size and drab color of these sediments are not conducive to preserving high quality paleomagnetic data (Figure S1). The Adamanian-Revueltian faunal transition occurs in the Jim Camp Wash beds of the Sonsela Member about 10 m above the base of The Peninsula section (Parker & Martz, 2011) which unfortunately is in this interval of ambiguous magnetic polarity data (Zeigler et al., 2017).

The 335-m-thick stratigraphic section of the Chinle Formation in core PFNP-1a is unconformably overlain by the Neogene Bidahochi Formation and unconformably overlies the Early-Middle Triassic Moenkopi Formation (Olsen et al., 2018). Magnetostratigraphic correlations to the N-H APTS have now been extended from those reported for the upper Chinle (Owl Rock, Petrified Forest and upper Sonsela members; Kent et al., 2018) to the lower Chinle (lower Sonsela, Blue Mesa, and Mesa Redondo members; this study). These correlations reflect two apparent sedimentary regimes. Proceeding upsection, the first regime encompasses the Mesa Redondo and Blue Mesa members and magnetozones PF10n (partim) to PF5r, which correlate to chrons E9n (partim) to E13r with an age range from ~224 to 216 Ma (based on the N-H APTS); this 85-m-thick interval of the lower Chinle accumulated at an average rate of ~10 m/Myr. At about the lower boundary of magnetozone PF5n at the 270 msd level and close to the base of the Sonsela Member, the sediment accumulation rate evidently more than triples to the ~34 m/Myr rate previously estimated for the upper Chinle Formation (Kent et al., 2018); this higher
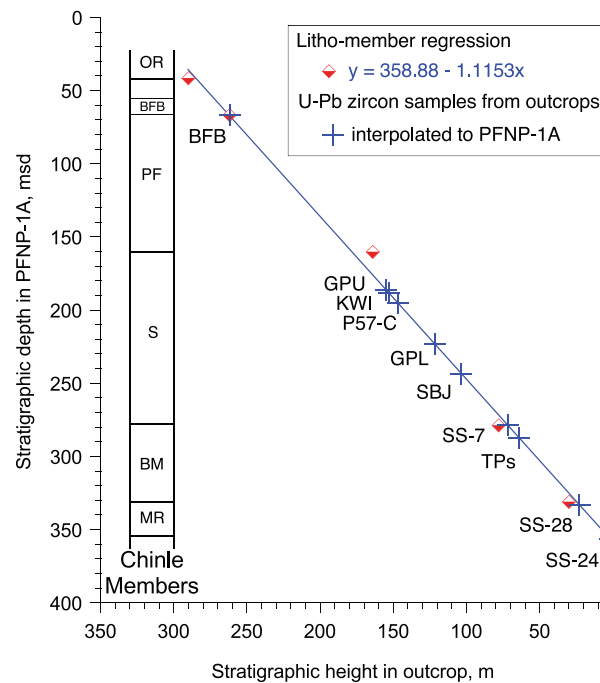
Figure 4. Depth registry to core PFNP-1A of lithostratigraphic members of Chinle Formation (OR, Owl Rock; PF, Petrified Forest with BFB, Black Forest Bed; S, Sonsela; BM, Blue Mesa; MR, Mesa Redondo) and levels of reported U-Pb samples in an outcrop composite section in and in the vicinity of Petrified Forest National Park (Atchley et al., 2013). Samples from outcrop with reported high-precision U-Pb detrital zircon ages were registered to meters stratigraphic depth (msd) in core PFNP-1A using the linear regression equation shown in the legend. See Tables S3 and S4 for listings and references.

average accumulation rate extends from magnetozones PF5n to PF1r that correlate to chrons E14n to within E17r with an age range of ~216 to ~209 Ma for this 250-m-thick section of the Chinle Formation. The inflection in the age-depth curve coincides with the transition from the mudstone-dominated Blue Mesa Member to the sandstone-dominated Sonsela Member with abundant extrabasinal sediments that is regarded by Martz and Parker (2010) and Marsh et al. (2019) as a significant shift in the depositional regime. The specific cause of the change remains unclear but may have been due to an increase in accommodation space (perhaps related to halokinesis; see references in Dickinson, 2018), a more robust sediment supply (Martz & Parker, 2010), or a particular combination of these or other factors that then persisted for millions of years.

A suite of maximum depositional ages inferred from high-precision U-Pb detrital zircon CA-TIMS dates have been reported for sedimentary samples from exposures of the various members of the Chinle Formation in PFNP and its vicinity (Atchley et al., 2013; Nordt et al., 2015; Ramezani et al., 2011). To register the outcrop samples in the stratigraphic framework of core PFNP-1A, we compared the stratigraphic levels of member boundaries of the Chinle Formation delineated in core PFNP-1A to those in a composite outcrop stratigraphic log from Atchley et al. (2013). There is good mutual agreement (Figure 4 and Table S3), which allowed us to use a linear regression to register the outcrop sample heights in the Atchley et al. (2013) composite to msd in core PFNP-1A (Table S4). Dates for outcrop samples from the Petrified Forest and the upper Sonsela members (BFB, KWI and P57-C from the northern part of PFNP, and GPU from the southern part of PFNP) agree closely with the integrated magnetochronology and U-Pb geochronology derived from the upper Chinle Formation in core PFNP-1A (Kent et al., 2018) (Figure 3). In stark contrast, U-Pb ages for outcrop samples from the lower Sonsela, Blue Mesa and Mesa Redondo members (GPL, SBJ, SS-7, and TPs from southern PFNP, and SS-28 and SS-24 from Hunt Valley, about 25 km southeast of PFNP), show an irregular depth-age trend and are consistently but variably older (by 3 to 6 Myr) than the preferred age-depth interpretation of the magnetochronology for the lower Chinle in PFNP-1A (Figure 3).

A contributing although not wholly satisfactory explanation for the discrepancy may stem from the longstanding difficulty in making reliable correlations in the fluvial facies of the Chinle Formation over long distances, especially from the northern to southern areas of PFNP, as discussed above for the apparent ~100-m-thick sampling gap in the Sonsela Member in the composite section of Steiner and Lucas (2000). Nonetheless, it is noteworthy that the U-Pb age for outcrop sample GPU from the upper Sonsela Member in southern PFNP agrees well with the U-Pb age for sample KWI also from the upper Sonsela Member but from northern PFNP (Ramezani et al., 2011). Moreover, it was possible to successfully integrate the U-Pb ages from these and other outcrop samples to those from core PFNP-1A to produce an internally consistent chronostratigraphy for the upper Chinle Formation (Figure 3; Kent et al., 2018).

A related possibility is that the thickness of the Sonsela Member may be abbreviated by a regional unconformity (Heckert & Lucas, 2002) or by multiple disconformities (Ramezani et al., 2011), whereby most of the time associated with deposition of the unit may not be represented by sedimentary rock. What strongly argues against this option is that the newly delineated base of magnetozone PF5n falls on the well-calibrated linear age-depth trend for the upper Chinle: the thickness of PF5n of 53.26 msd and duration of correlative chron E14n of 1.24 Myr yields an average sediment accumulation rate of ~43 m/Myr. This interval rate is even higher than the overall average of 34 m/Myr for the upper Sonsela and the Petrified Forest members, providing even less reason to introduce one or more arbitrary unconformities within the Sonsela Member.

Extrapolating the 34 m/Myr average sediment accumulation rate down from the base of the Sonsela Member and magnetozone PF5n (=chron E14n) would imply that the underlying Blue Mesa, Mesa Redondo Member, and the base of the Chinle Formation (355 msd) are no older than ~218.5 Ma. In this unlikely circumstance, the expectation would be to find only the equivalent of chron E13r and especially E13n in this lowermost 85-m-thick section of the Blue Mesa and Mesa Redonda members. Instead, we find 10 credible polarity magnetozones, where magnetozone PF7r, which is the thickest magnetozone (22.21 m) below PF5n in this section, is a logical correlative to chron E11r, the longest polarity interval (at 2.01 Myr) in the N-H APTS older than E14r and which has been verified as correlative to PF4r by concordant U-Pb dates in core PFNP-1A (Figure 3; Kent et al., 2018). This provides a rationale for the magnetostratigraphic correlation of magnetozone sequence PF5r to PF10n to chron sequence E13r to E9n that yields an average sediment accumulation rate of ~10 m/Myr for the Blue Mesa and Mesa Redonda members. The only polarity interval missing with this correlation scheme is chron E13n.1r, whose duration is only 40 kyr. This makes it one of the shortest polarity intervals in the entire N-H APTS and thus most readily inadvertently skipped given the nominal meter-scale (or ~40 kyr for overall sediment accumulation rate of 22 m/Myr) sampling density for the Chinle Formation in core PFNP-1A.

4. Implications of the Magnetochronology for U-Pb Geochronology

The consistency of the magnetochronology down to the base of PF5n makes a strong case that high-precision U-Pb detrital zircon dates in samples from above the base of the Sonsela Member that are significantly older than 216.16 Ma, the onset of correlative chron E14n, have anomalously old maximum depositional ages. Foremost is outcrop sample GPL (218.02±0.28 Ma) from within the Sonsela Member (Ramezani et al., 2011) that is projected in core PFNP-1A to just ~10 m below the base of magnetozone PF4r, correlative to the onset of chron E14r at 214.92 Ma according to the N-H APTS (Figure 3). Taken at face value, the apparent 3 Myr difference in age over such a small stratigraphic interval would imply an intervening unconformity or at least a drastically reduced net sediment accumulation of only 0.3 m/Myr, about two orders of magnitude less than estimated for the rest of the Sonsela Member as well as the overlying Petrified Forest Member. On similar grounds, outcrop sample SBJ (219.32±0.27 Ma) from the Sonsela Member (Ramezani et al., 2011) would also be suspect as anomalously old, as would SS-7 (220.12±0.07 Ma; (Atchley et al., 2013) and TPs (223.04±0.27 Ma; Ramezani et al., 2011) from the uppermost Blue Mesa Member, although judgment can be deferred on samples SS-28 (225.18±0.28 Ma; Ramezani et al., 2011) and SS-24 (227.60±0.08 Ma; Atchley et al., 2013) from the Mesa Redonda Member because they come from distant Hunt Valley with less certain lithostratigraphic ties to core PFNP-1A.

What we regard as anomalously old U-Pb detrital zircon ages evidently reflect bias from recycled zircons due to the lack of an adequate juvenile zircon population, either missing due to the absence of depositional age-equivalent volcanic air fall zircons reaching the area of deposition or by the failure to find a sufficient

number in a sample for detailed U-Pb CA-TIMS analyses. On the other end of the age spectrum, residual Pb-loss is a potential confounding issue for identifying zircons closest to depositional age, as evidenced by populations of carefully selected zircons that still contain one or more anomalously young CA-ID-TIMS dated zircons, for example, samples 52Q-2, 158Q-2, and 177Q-1 (Kent et al., 2018). It remains to fully understand and diagnose why the high-precision U-Pb detrital zircon dates from the lower Sonsela and upper Blue Mesa members tend to be dominated by recycled zircons and give anomalously old (by ~3 Myr or more) dates compared to the magnetochronology, which in the upper Sonsela and Petrified Forest Members is in excellent agreement with dates from both outcrop and core PFNP-1A (Figure 3). The problem might be addressed by sampling mudstones besides the usual sandstones to increase the probability of finding contemporaneous air fall (juvenile) zircons and address the possibility that there were only sporadic million-year-scale bursts of volcanic activity that account for the zircon age distribution in samples from the Chinle Formation in Petrified Forest National Park.

The aforementioned uncertainty in the age model for the lower Chinle Formation has implications for the timing of the Adamanian-Revueltian land vertebrate faunal zone boundary. The Adamanian-Revueltian transition has traditionally been placed within the Sonsela Member, near the base of the so-called Sonsela sandstone bed (=Jasper Forest bed; Lucas, 1998) or several meters above this bed in the lower part of the Jim Camp Wash beds (Martz & Parker, 2010). A marked palynozonal transition (Zone II to Zone III) occurs at about the same stratigraphic level within the Sonsela Member (Baranyi et al., 2018; Reichgelt et al., 2013). According to Ramezani et al. (2011), a conservative constraint for the Adamanian-Revueltian boundary would be between their samples SBJ (approximately 219 Ma) and GPU (approximately 213 Ma; Figure 3). The ~213 Ma age for sample GPU is in excellent accord with our integrated chronostratigraphy of the upper Chinle Formation (Kent et al., 2018). However, we already made the argument based on magnetochronology that the Sonsela Member (along with the Adamanian-Revueltian transition) is no older than 216.16 Ma (Figure 3), which implies that the reported U-Pb age for sample SBJ from the Sonsela Member is at least 3 Myr older than its projected depositional age.

Based on our magnetochronology, the timing of the Manicouagan impact crater in Quebec, Canada (quoted U-Pb zircon date of 215.5 Ma (Ramezani et al., 2005)), whose melt rocks record normal geomagnetic polarity (Eitel et al., 2016) most probably of chron E14n (Kent et al., 2017), would correspond to the middle of magnetozone PF5n in core PFNP-1A and be within the updated age constraints on the Adamanian-Revueltian boundary (~216 to 213 Ma). The temporal correlation is still too broad to make a compelling case for a causal relationship between the impact and the biotic change, which is nonetheless not precluded. The estimated age range of the Adamanian-Revueltian boundary would also occupy about the same time interval as the Neshanichian land vertebrate age and the transition between the New Oxford-Lockatong and Lower Passaic-Heidlersburg sporomorph zones of the Newark rift basins of eastern North America, all correlating to within the marine Alaunian Sub-Stage of the Norian (Kent et al., 2017; Maron et al., 2019).

In the Southern Hemisphere, magnetochronology of the Los Colorados Formation of the Ischigualasto-Villa Union basin in Argentina shows that the continental red bed unit extends from chron E7r at an estimated age of 227 Ma, which is close to the age of the Carnian-Norian boundary, to its erosional upper surface in E15n at ~213 Ma (Kent et al., 2014). The ~500-m-thick nonmarine Los Colorados Formation thus encompasses about 14 million years of Late Triassic time and was deposited at an average rate of ~35 m/Myr. The La Esquina dinosaur-bearing fauna from the upper part of the Los Colorados Formation (Martínez et al., 2011), projected to be ~213 Ma from the magnetochronology (Kent et al., 2014), may thus be of similar age as the earliest part of the Revueltian land vertebrate faunal zone in the Chinle Formation.

5. Conclusions

We suggest that the magnetochronology of the 335-m-thick section of the Chinle Formation recovered in core PFNP-1A is essentially complete to well within the resolution of the 405 kyr astronomical cycle used to calibrate the N-H APTS. The total age range of ~224 to 209 Ma (from within correlative chrons E9n to E17r, respectively) makes the Chinle Formation in PFNP entirely of Norian age (205.5–227 Ma; Wotzlaw et al., 2014; Maron et al., 2019)), as previously suggested (e.g., Olsen et al., 2011; Ramezani et al., 2011). The average sediment accumulation rate for the entire Chinle is ~22 m/Myr but is not always uniform from member to member. Instead, there is an up-section increase in sediment accumulation rate at around 216 Ma

from ~10 m/Myr in the Mesa Redondo and Blue Mesa members to ~34 m/Myr in the Sonsela and Petrified Forest members. The increase coincides with a significant shift in the depositional regime from the mudstone-dominated Blue Mesa Member to the sandstone-dominated Sonsela Member (Martz & Parker, 2010). The magnetochronology is also supportive of further studies to narrow the apparent temporal association of the Adamanian-Revueltian biotic transition and the Zone II to Zone III palynofloral boundary within the Sonsela Member with the Manicougan impact (Parker & Martz, 2011; Zeigler et al., 2017).

Our preferred interpretation of the magnetochronology of the Chinle Formation in core PFNP-1A is ostensibly at odds with the reported high-precision U-Pb detrital zircon dates from outcrop sections of the lower Sonsela, Blue Mesa, and possibly the Mesa Redondo members, which by comparison are anomalously old (by ~3 Myr or more). From the sample descriptions, all the U-Pb detrital zircon dates under discussion from the Chinle Formation in outcrop (Atchley et al., 2013; Ramezani et al., 2011) as well as core PFNP-1A (Kent et al., 2018) are from laterally transported and reworked siltstones and sandstones, which is why the U-Pb detrital zircon dates are regarded as maximum depositional ages. The puzzle is why the maximum depositional ages agree closely with the magnetochronology in the upper Sonsela and Petrified Forest members but tend to be irregularly older by several million years than the magnetochronology in the lower Sonsela and Blue Mesa members. If accepted as providing ages that are close to times of deposition, closely spaced samples GPL and GPU with divergent ages would require an unconformity (or at least a radical reduction in sediment accumulation rate) spanning about 3 Myr within the Sonsela Member as well as much more complicated correlation of the magnetostratigraphy to the N-H APTS. The Adamanian-Revueltian transition would fall within the hypothetical unconformity and could then represent a truncated record of a more gradual faunal change. While such alternative interpretations are not necessarily precluded, there is no supporting physical evidence of a long hiatus, such as a gross change in sediment character, within the Sonsela Member or by the paleomagnetic polarity stratigraphy reported here.

Sandstones often contain detrital zircons with a broad range of ages that are the basis for provenance studies (e.g., Dickinson & Gehrels, 2009; Riggs et al., 1996). In chronostratigraphic applications, recycled zircons need to be distinguished from juvenile (air-fall) zircons that ideally are supplied continuously from regional volcanism and can thus provide maximum depositional ages that converge with the time of deposition of the enclosing sediment. The distinction of recycled and juvenile zircons may not always be readily established in a sample population, especially when a dominant recycled phase is only a few million years older than the depositional age and there is only a small juvenile component. In the case of the Chinle Formation, particularly the lower part of the unit, the available age data could be at least partly explained by just a few major episodes of volcanic products reaching the area starting between ~224 and 220 Ma, with the introduced zircons recycled until another burst of volcanic products reached the area between ~214 and 213 Ma (and then again at around 210 Ma), each time supplying another population of juvenile zircons for recycling. Ongoing CA-TIMS (Rasmussen et al., 2017) and LA-ICPMS (Gehrels et al., 2019) U-Pb detrital zircon studies of samples from core PFNP-1A are not inconsistent with such a model and our preferred magnetochronology, but also offer alternative interpretations of the data.

References

Atchley, S. C., Nordt, L. C., Dworkin, S. I., Ramezani, J., Parker, W. G., Ash, S. R., & Bowring, S. A. (2013). A linkage among Pangean tectonism, cyclic alluviation, climate change, and biologic turnover in the Late Triassic: The record from the Chinle Formation, southwestern United States. *Journal of Sedimentary Research*, *83*(12), 1147–1161. https://doi.org/10.2110/jsr.2013.89

Baranyi, V., Reichgelt, T., Olsen, P. E., Parker, W. G., & Kürschner, W. M. (2018). Norian vegetation history and related environmental changes: New data from the Chinle Formation, Petrified Forest National Park (Arizona, SW USA). *Geological Society of America Bulletin*, *130*(5-6), 775–795. https://doi.org/10.1130/B31673.1

Dickinson, W. R. (2018). Tectonosedimentary relations of pennsylvanian to Jurassic Strata on the Colorado Plateau. *Geological Society of America Special Papers*, *533*, 1–184. https://doi.org/10.1130/2018.2533

Dickinson, W. R., & Gehrels, G. E. (2009). Use of U–Pb ages of detrital zircons to infer maximum depositional ages of strata: A test against a Colorado Plateau Mesozoic database. *Earth and Planetary Science Letters*, *288*(1–2), 115–125. https://doi.org/10.1016/j.epsl.2009.09.013

Eitel, M., Gilder, S. A., Spray, J., Thompson, L., & Pohl, J. (2016). A paleomagnetic and rock magnetic study of the Manicouagan impact structure: Implications for crater formation and geodynamo effects. *Journal of Geophysical Research: Solid Earth*, *121*, 436–454. https://doi.org/10.1002/2015JB012577

Gehrels, G. E., D. Giesler, P. E. Olsen, D. V. Kent, A. Marsh, W. G. Parker, et al. (2019), LA-ICPMS U-Pb geochronology of detrital zircon grains from the Chinle Formation (Colorado Plateau Coring Project), paper 65-8 presented at the GSA 2019 Fall meeting, Phoenix.

Heckert, A. B., & Lucas, S. G. (2002). Revised Upper Triassic stratigraphy of the Petrified Forest National Park, Arizona, U.S.A. *Bulletin of the New Mexico Museum of Natural History and Science*, *21*, 1–36.

Hinnov, L. A. (2018). Astronomical metronome of geological consequence. *Proceedings of the National Academy of Sciences*, *115*(24), 6104–6106. https://doi.org/10.1073/pnas.1807020115

Kent, D. V., & Irving, E. (2010). Influence of inclination error in sedimentary rocks on the Triassic and Jurassic apparent polar wander path for North America and implications for Cordilleran tectonics. *Journal of Geophysical Research*, *115*, B10103. https://doi.org/10.1029/12009JB007205

Kent, D. V., Olsen, P. E., & Muttoni, G. (2017). Astrochronostratigraphic polarity time scale (APTS) for the Late Triassic and Early Jurassic from continental sediments and correlation with standard marine stages. *Earth-Science Reviews*, *166*, 153–180. https://doi.org/10.1016/j.earscirev.2016.12.014

Kent, D. V., Olsen, P. E., Rasmussen, C., Lepre, C., Mundil, R., Irmis, R. B., et al. (2018). Empirical evidence for stability of the 405-kiloyear Jupiter-Venus eccentricity cycle over hundreds of millions of years. *Proceedings of the National Academy of Sciences*, *115*(24), 6153–6158. https://doi.org/10.1073/pnas.1800891115

Kent, D. V., Malnis, P. S., Colombi, C. E., Alcober, O. A., & Martínez, R. N. (2014). Age constraints on the dispersal of dinosaurs in the Late Triassic from magnetochronology of the Los Colorados Formation (Argentina). *Proceedings of the National Academy of Sciences*, *111*(22), 7958–7963. https://doi.org/10.1073/pnas.1402369111

Kent, D. V., & Tauxe, L. (2005). Corrected Late Triassic latitudes for continents adjacent to the North Atlantic. *Science*, *307*(5707), 240–244. https://doi.org/10.1126/science.1105826

Kirschvink, J. L. (1980). The least-squares line and plane and the analysis of palaeomagnetic data. *Geophysical Journal of the Royal Astronomical Society*, *62*(3), 699–718. https://doi.org/10.1111/j.1365-246X.1980.tb02601.x

Lucas, S. G. (1998). Global Triassic tetrapod biostratigraphy and biochronology. *Palaeogeography, Palaeoclimatology, Palaeoecology*, *143*(4), 347–384. https://doi.org/10.1016/S0031-0182(98)00117-5

Maron, M., Muttoni, G., Rigo, M., Gianolla, P., & Kent, D. V. (2019). New magnetobiostratigraphic results from the Ladinian of the Dolomites and implications for the Triassic geomagnetic polarity timescale. *Palaeogeography, Palaeoclimatology, Palaeoecology*, *517*, 52–73. https://doi.org/10.1016/j.palaeo.2018.11.024

Marsh, A. D., Parker, W. G., Stockli, D. F., & Martz, J. W. (2019). Regional correlation of the Sonsela Member (Upper Triassic Chinle Formation) and detrital U-Pb zircon data from the Sonsela Sandstone bed near the Sonsela Buttes, northeastern Arizona, USA, support the presence of a distributive fluvial system. *Geosphere*, *15*, 1–12. https://doi.org/10.1130/GES02004.02001

Martínez, R. N., Sereno, P. C., Alcober, O. A., Colombi, C. E., Renne, P. R., Montañez, I. P., & Currie, B. S. (2011). A basal dinosaur from the dawn of the dLithostratigraphy of the Sonselainosaur era in southwestern Pangaea. *Science*, *331*(6014), 206–210. https://doi.org/10.1126/science.1198467

Martz, J. W., & Parker, W. G. (2010). Revised lithostratigraphy of the Sonsela Member (Chinle Formation, Upper Triassic) in the southern part of Petrified Forest National Park, Arizona. *PLoS ONE*, *5*(2), e9329. https://doi.org/10.1371/journal.pone.0009329

Martz, J. W., & Parker, W. G. (2017). Revised formulation of the Late Triassic land vertebrate "Faunachrons" of western North America: Recommendations for codifying nascent systems of vertebrate biochronology. In K. E. Zeigler, & W. G. Parker (Eds.), *Terrestrial Depositional Systems*, (pp. 39–124). Amsterdam: Elsevier.

Nordt, L., Atchley, S., & Dworkin, S. (2015). Collapse of the Late Triassic megamonsoon in western equatorial Pangea, present-day American Southwest. *Geological Society of America Bulletin*, *127*(11-12), 1798–1815. https://doi.org/10.1130/B31186.1

Olsen, P. E., Geissman, J. W., Kent, D. V., Gehrels, G. E., Mundil, R., Irmis, R. B., et al., & the CPCD team (2018). Colorado Plateau Coring Project, Phase I (CPCP-I): A continuously cored, globally exportable chronology of Triassic continental environmental change from western North America. *Scientific Drilling*, *24*, 15–40. https://doi.org/10.5194/sd-24-15-2018

Olsen, P. E., Kent, D. V., & Whiteside, J. H. (2011). Implications of the Newark Supergroup-based astrochronology and geomagnetic polarity time scale (Newark-APTS) for the tempo and mode of the early diversification of the Dinosauria. *Earth and Environmental Science Transactions of the Royal Society of Edinburgh*, *101*, 201–229.

Parker, W. G., & Martz, J. W. (2011). The Late Triassic (Norian) Adamanian–Revueltian tetrapod faunal transition in the Chinle Formation of Petrified Forest National Park, Arizona. *Earth and Environmental Science Transactions of the Royal Society of Edinburgh*, *101*(Special Issue 3-4), 231–260.

Ramezani, J., Bowring, S. A., Pringle, M. S., Winslow, F. D., & Rasbury, E. T. (2005). The Manicouagan impact melt rock: A proposed standard for the intercalibration of U-Pb and ^{40}Ar/^{39}Ar isotopic systems. *Geochimica et Cosmochimica Acta*, *69*, A321.

Ramezani, J., Hoke, G. D., Fastovsky, D. E., Bowring, S. A., Therrien, F., Dworkin, S. I., et al. (2011). High-precision U-Pb zircon geochronology of the Late Triassic Chinle Formation, Petrified Forest National Park (Arizona, USA): Temporal constraints on the early evolution of dinosaurs. *Geological Society of America Bulletin*, *123*(11-12), 2142–2159. https://doi.org/10.1130/B30433.1

Rasmussen, C., Mundil, R., Irmis, R. B., Keller, B., Giesler, D., Gehrels, G. E., & CPCP Science Party (2017). U-Pb geochronology of non-marine Upper Triassic strata of the Colorado Plateau (western North America): Implications for stratigraphic correlation and paleoenvironmental reconstruction, paper PP44A-04 presented at AGU 2017 Fall Meeting, New Orleans.

Reichgelt, T., Parker, W. G., Martz, J. W., Conran, J. G., Cittert, J. H. A. v. K.-v., & Kürschner, W. M. (2013). The palynology of the Sonsela Member (Late Triassic, Norian) at Petrified Forest National Park, Arizona, USA. *Review of Palaeobotany and Palynology*, *189*, 18–28. https://doi.org/10.1016/j.revpalbo.2012.11.001

Riggs, N. R., Lehman, T. M., Gehrels, G. E., & Dickinson, W. R. (1996). Detrital zircon link between headwaters and terminus of the Upper Triassic Chinle-Dockum paleoriver system. *Science*, *273*(5271), 97–100. https://doi.org/10.1126/science.273.5271.97

Steiner, M. B., & Lucas, S. G. (2000). Paleomagnetism of the Late Triassic Petrified Forest Formation, Chinle Group, western United States: Further evidence of "large" rotation of the Colorado Plateau. *Journal of Geophysical Research*, *105*(B11), 25,791–25,808. https://doi.org/10.1029/2000JB900093

Wotzlaw, J.-F., Guex, J., Bartolini, A., Gallet, Y., Krystyn, L., McRoberts, C. A., et al. (2014). Towards accurate numerical calibration of the Late Triassic: High-precision U-Pb geochronology constraints on the duration of the Rhaetian. *Geology*, *42*(7), 571–574. https://doi.org/10.1130/G35612.1

Zeigler, K. E., Parker, W. G., & Martz, J. W. (2017). The lower Chinle Formation (Late Triassic) at Petrified Forest National Park, Southwestern USA: A case study in magnetostratigraphic correlations. In K. E. Zeigler, & W. G. Parker (Eds.), *Terrestrial Depositional Systems Deciphering Complexities through Multiple Stratigraphic Methods*, edited by, (pp. 251–293). Amsterdam, Netherlands: Elsevier.

@AGUPUBLICATIONS

Geochemistry, Geophysics, Geosystems

Supporting Information for

Magnetochronology of the entire Chinle Formation (Norian age) in a scientific drill core from Petrified Forest National Park (Arizona, USA) and implications for regional and global correlations in the Late Triassic

Dennis V. Kent[1,2], Paul E. Olsen[2], Christopher Lepre[1,2], Cornelia Rasmussen[3,4],

Roland Mundil[5], George E. Gehrels[6], Dominique Giesler[6], Randall B. Irmis[3,7],

John W. Geissman[8], William G. Parker[9]

[1]Earth & Planetary Sciences, Rutgers University, Piscataway, NJ 08854

[2]Lamont-Doherty Earth Observatory of Columbia University, Palisades, NY 10964

[3]Department of Geology & Geophysics, University of Utah, Salt Lake City, UT 84112

[4]Institute for Geophysics, Jackson School of Geosciences, University of Texas at Austin, TX 78758

[5]Berkeley Geochronology Center, 2455 Ridge Rd., Berkeley CA 94709

[6]Department of Geosciences, University of Arizona, Tucson, AZ 85721

[7]Natural History Museum of Utah, University of Utah, Salt Lake City, UT 84108

[8]Department of Geosciences, University of Texas at Dallas, Richardson, TX 75080

[9]Petrified Forest National Park, Petrified Forest, AZ 86028

Contents of this file

Figure S1. Lithostratigraphy of the Chinle Formation (and upper Moenkopi Formation) as exposed in Petrified Forest National Park (after *Martz and Parker,* 2010) showing the stratigraphic intervals represented by the magnetostratigraphic study of *Steiner and Luca* [2000] from sampling in the northern (upper section) and southern (lower section) PFNP (see text for discussion and references of correlations) and the composite magnetostratigraphy based on three contiguous sections (Tepee, Blue Mesa and The Peninsula, with possibly a meter or two of stratigraphic overlap between the sections) in southern PFNP by *Zeigler et al.* [2017]. Modified from Figure 2 in *Zeigler et al.* [2017] by placing all sections on same thickness scale as indicated by scale bar at top of figure and equivalent scale next to composite magnetostratigraphy, and following section correlations and thicknesses given in Figure 3 of *Zeigler et al.* [2017]. Main points of correlation of magnetostratigraphic sections to lithostratigraphy are Black Forest Bed (BFB) at top of upper section of *Steiner and Luca* [2000], Sonsela/Blue Mesa (BM) member contact in lower section of *Steiner and Luca* [2000] as well as in Blue Mesa section of composite of *Zeigler et al.* [2017]. PF is Petrified Forest Member and MR is Mesa Redondo Member of Chinle Formation. Polarity columns show black for normal polarity, white for reverse polarity, open with no lateral bounds for unsampled intervals, gray for sampled intervals with uninterpretable polarity, and black and white half-bars are for single sample-level normal and reverse polarity intervals. Magnetic polarity correlations between the composite section of *Zeigler et al.* [2017]) and the lower section of *Steiner and Luca* [2000] are poor overall although the *Steiner and Luca* [2000] sections can be correlated to the N-H APTS (see **Fig. 3**).

Table S1. Principal component analysis of thermal demagnetization of NRM of samples from PFNP-1A.

mcd	msd	ID	n	MAD	bDec	bInc	bLon	bLat	rbLon	rbLat	T1	T2	Notes
279.09	241.70	222Q1.52	5	10	349.2	46.5	124.7	78.3	248.6	73.0	300	600	PF5n
280.68	243.08	223Q1.58	5	3	8.1	19.5	51.8	63.9	345.0	73.1	300	600	"
281.27	243.59	224Q1.56	5	11	59.2	59.1	315.8	43.6	304.9	23.6	300	600	"
282.79	244.90	225Q2.50	6	16	8.2	20.2	51.4	64.2	343.7	73.0	150	600	"
283.70	245.69	226Q1.55	5	7	301.6	25.5	153.1	33.4	172.2	41.8	300	600	"
283.92	245.88	226Q2.08	5	7	359.4	13.3	71.5	61.6	9.3	80.7	300	600	"
285.61	247.35	227Q3.03	5	5	341.9	23.9	110.6	62.1	175.2	81.0	300	600	"
288.23	*249.61*	*229Q1.51*	*5*	*31*	*330.7*	*7.0*	*117.5*	*48.4*	*145.2*	*68.6*	*300*	*600*	*MAD*
288.97	250.26	229Q2.52	5	3	23.2	-0.4	33.6	48.6	0.8	56.1	300	600	"
289.57	250.77	230Q1.33	5	2	11.2	5.4	49.9	56.0	4.4	68.3	300	600	"
290.07	*251.21*	*230Q2.29*	*5*	*28*	*334.6*	*38.4*	*135.8*	*64.0*	*200.4*	*71.0*	*300*	*600*	*MAD*
291.17	252.16	231Q1.40	5	3	52.4	-11.8	9.0	25.9	356.2	26.5	300	600	"
291.76	252.67	231Q2.28	5	5	35.8	-16.0	25.1	35.1	5.1	41.5	300	600	"
292.50	253.31	232Q1.21	5	1	12.0	11.2	46.8	58.6	356.1	68.5	300	600	"
293.19	253.91	232Q2.22	5	2	0.1	12.3	70.0	61.1	10.2	79.8	300	600	"
294.11	254.71	233Q1.30	5	3	341.0	25.0	112.9	62.1	178.0	80.0	300	600	"
294.94	255.43	233Q2.40	5	9	9.4	26.4	46.0	67.2	332.2	71.7	300	600	"
295.54	255.95	234Q1.20	5	11	353.1	20.0	86.1	64.4	357.9	87.8	300	600	"
296.31	256.61	234Q2.26	7	12	352.0	33.0	94.8	71.5	262.0	82.8	300	650	"
297.15	*257.34*	*235Q1.29*	*5*	*7*	*330.1*	*62.6*	*190.5*	*65.5*	*229.1*	*52.3*	*300*	*600*	*ovpr*
298.05	*258.12*	*235Q2.42*	*5*	*17*	*121.6*	*2.9*	*319.5*	*-24.5*	*332.8*	*-39.4*	*300*	*600*	*MAD*
300.11	259.90	238Q1.51	5	2	16.0	4.2	42.4	53.8	1.4	63.6	300	600	"
300.77	260.47	238Q2.40	5	11	331.8	17.3	121.5	53.2	159.5	71.1	300	600	"
302.30	*261.80*	*239Q1.56*	*5*	*22*	*151.6*	*1.0*	*293.0*	*-45.6*	*314.5*	*-67.7*	*300*	*600*	*MAD*
302.68	*262.13*	*239Q2.19*	*5*	*17*	*304.6*	*37.7*	*159.5*	*39.8*	*182.9*	*44.5*	*300*	*600*	*MAD*
303.46	262.80	240Q1.20	5	13	335.0	14.9	115.9	54.2	153.4	73.9	300	600	"
304.39	263.61	240Q2.43	5	14	355.9	0.7	77.4	55.1	48.3	78.4	300	600	"
304.62	*263.81*	*240Q3.14*	*5*	*29*	*233.8*	*-7.3*	*179.8*	*-31.3*	*165.3*	*-27.3*	*300*	*600*	*MAD*
305.00	264.14	241Q1.21	6	7	23.8	26.1	19.1	59.8	335.2	57.8	300	625	"
306.05	265.05	241Q2.52	5	7	7.1	29.0	50.4	69.4	325.7	73.6	300	600	"
306.49	265.43	242Q1.18	5	2	354.8	44.1	97.4	79.7	267.0	74.6	300	600	"
306.99	265.86	242Q2.19	5	2	352.5	43.4	105.7	78.3	259.5	75.5	300	600	"
307.40	266.22	242Q3.11	5	3	20.9	37.7	12.0	67.0	320.4	59.5	300	600	"
308.15	*266.87*	*243Q1.32*	*5*	*21*	*159.9*	*-30.2*	*298.9*	*-64.0*	*11.6*	*-78.0*	*300*	*600*	*MAD*
308.96	*267.57*	*243Q2.44*	*5*	*29*	*144.0*	*60.0*	*276.8*	*-7.1*	*277.8*	*-32.6*	*300*	*600*	*MAD*
309.73	268.23	244Q1.37	5	2	4.5	13.5	60.8	61.5	359.4	76.0	300	600	"
310.01	268.48	244Q2.10	7	15	343.8	5.7	98.8	54.4	115.8	79.3	300	650	PF5n
311.24	269.54	245Q1.36	5	3	217.0	18.7	205.0	-33.3	186.2	-39.8	300	600	PF5r
311.91	270.12	245Q2.37	5	2	183.1	2.6	245.0	-53.5	208.2	-72.8	300	600	"
312.89	270.97	246Q1.49	5	10	178.4	29.9	252.2	-38.8	238.3	-62.1	300	600	"
314.31	*272.20*	*247Q1.38*	*5*	*24*	*45.4*	*-20.4*	*18.2*	*27.4*	*3.6*	*31.8*	*300*	*600*	*MAD*
314.88	272.69	247Q2.31	5	9	183.4	59.5	247.5	-14.5	241.8	-37.5	300	600	"
316.70	274.27	248Q2.58	5	8	153.7	-11.1	295.7	-51.8	328.1	-72.2	300	600	"
317.22	*274.72*	*249Q1.24*	*5*	*16*	*199.9*	*-34.5*	*197.5*	*-66.1*	*144.2*	*-60.9*	*300*	*600*	*MAD*
317.96	*275.36*	*249Q2.33*	*5*	*16*	*21.7*	*45.7*	*357.5*	*69.8*	*310.1*	*56.8*	*300*	*600*	*MAD*
319.02	*276.28*	*250Q1.52*	*5*	*17*	*99.1*	*63.4*	*297.6*	*18.3*	*296.3*	*-4.8*	*300*	*600*	*MAD*
319.71	*276.88*	*250Q3.37*	*5*	*32*	*318.4*	*22.5*	*138.8*	*45.7*	*168.6*	*58.1*	*300*	*600*	*MAD*
320.52	*277.58*	*251Q1.50*	*5*	*21*	*265.5*	*-29.4*	*149.7*	*-12.6*	*147.5*	*1.4*	*300*	*600*	*MAD*

322.32	*279.14*	*252Q2.15*	*5*	*24*	*189.2*	*83.4*	*248.0*	*22.2*	*249.8*	*-1.5*	*300*	*600*	*MAD*
322.34	279.15	252Q2.17	5	1	101.9	-0.4	333.5	-9.8	339.9	-20.6	300	600	"
323.70	280.33	253Q1.63	7	3	90.8	51.6	312.5	17.3	310.3	-2.4	300	600	"
324.24	280.80	253Q2.47	7	7	208.1	32.9	218.8	-30.7	201.6	-43.4	300	600	"
325.53	281.92	254Q2.27	4	3	4.2	7.9	62.1	58.6	10.5	75.2	300	525	
327.03	283.22	255Q2.24	7	1	206.3	-32.1	190.5	-60.7	148.9	-55.1	300	600	PF5r
329.01	284.93	256Q2.67	7	9	32.6	19.6	12.3	51.2	340.9	49.0	300	600	PF6n
330.45	*286.18*	*257Q2.62*	*7*	*22*	*86.7*	*-8.4*	*345.6*	*0.3*	*346.9*	*-6.5*	*300*	*600*	
331.98	287.50	258Q3.30	7	5	23.8	10.1	28.5	52.8	351.3	57.0	300	600	"
332.77	288.19	260Q1.40	7	5	358.5	8.3	73.1	59.1	25.0	80.0	300	600	"
333.33	288.67	260Q2.21	7	7	337.6	3.6	107.2	50.7	130.4	74.0	300	600	"
334.38	*289.58*	*261Q1.64*	*7*	*18*	*185.1*	*18.3*	*243.0*	*-45.3*	*218.5*	*-65.3*	*300*	*600*	*MAD*
335.06	290.17	262Q1.41	7	3	2.7	14.9	64.4	62.4	358.6	77.9	300	600	"
336.68	291.57	263Q2.50	7	3	5.1	57.7	300.2	84.8	276.2	59.7	300	600	"
336.97	*291.82*	*264Q1.18*	*7*	*22*	*18.0*	*71.0*	*275.9*	*66.2*	*273.7*	*40.6*	*300*	*600*	*MAD*
338.17	292.86	265Q1.47	7	4	353.9	-2.3	80.4	53.3	59.8	77.6	300	600	"
338.43	293.09	265Q2.25	7	4	10.8	5.6	50.5	56.2	4.6	68.7	300	600	"
339.03	293.61	265Q3.35	7	11	352.6	10.4	84.8	59.4	57.3	84.1	300	600	"
339.66	294.15	266Q1.43	7	3	350.6	33.9	99.4	71.5	251.5	82.3	300	600	PF6n
340.19	*294.61*	*267Q1.35*	*7*	*27*	*183.1*	*-17.3*	*243.3*	*-63.6*	*172.2*	*-77.8*	*300*	*600*	*MAD*
340.94	295.26	267Q2.34	7	6	206.4	4.7	211.2	-45.1	182.3	-52.3	300	600	PF6r
341.96	296.15	268Q1.60	7	2	169.1	5.6	267.6	-50.7	261.5	-76.2	300	600	"
342.13	*296.29*	*268Q2.05*	*7*	*30*	*347.1*	*51.2*	*147.2*	*78.8*	*244.9*	*68.7*	*300*	*600*	*MAD*
343.68	*297.64*	*270Q1.64*	*7*	*19*	*260.1*	*73.7*	*216.9*	*25.2*	*223.1*	*8.9*	*300*	*600*	*MAD*
343.95	297.87	270Q2.23	7	6	197.7	40.9	231.6	-29.1	216.6	-46.9	300	600	"
344.84	*298.64*	*271Q1.43*	*7*	*2*	*153.5*	*77.0*	*261.2*	*12.4*	*261.2*	*-12.8*	*300*	*600*	*ovpr*
345.58	299.28	271Q2.47	7	8	155.8	29.9	278.6	-33.9	283.2	-59.2	300	600	PF6r
346.30	299.90	272Q1.37	7	3	338.2	19.2	113.7	57.9	160.5	77.4	300	600	PF7n
346.40	299.99	272Q2.06	7	2	2.8	-0.9	65.4	54.4	26.9	73.7	300	600	"
348.30	301.64	273Q2.45	7	0	356.6	9.8	76.9	59.7	29.9	81.8	300	600	PF7n
349.10	302.33	274Q1.43	7	0	123.6	-24.7	331.3	-34.8	351.4	-43.7	300	600	PF7r
349.49	302.67	274Q2.12	7	4	123.4	30.7	306.4	-15.6	314.2	-35.6	300	600	"
352.22	*305.03*	*276Q1.50*	*7*	*8*	*23.3*	*59.2*	*318.4*	*70.9*	*292.7*	*49.8*	*300*	*600*	*bit*
352.84	*305.57*	*276Q2.40*	*7*	*6*	*1.4*	*42.8*	*63.1*	*79.7*	*287.8*	*72.8*	*300*	*600*	*bit*
353.87	*306.46*	*277Q1.62*	*7*	*1*	*5.9*	*1.6*	*59.8*	*55.3*	*16.9*	*72.0*	*300*	*600*	*bit*
354.53	*307.03*	*277Q2.58*	*7*	*1*	*177.7*	*4.0*	*254.0*	*-52.8*	*225.8*	*-75.5*	*300*	*600*	*bit*
354.98	*307.42*	*278Q1.21*	*7*	*3*	*6.0*	*17.6*	*56.9*	*63.4*	*349.6*	*75.0*	*300*	*600*	*bit*
355.80	*308.13*	*278Q2.28*	*7*	*4*	*28.3*	*37.6*	*2.2*	*61.5*	*323.2*	*52.8*	*300*	*600*	*bit*
356.87	*309.06*	*279Y2.40*	*7*	*5*	*8.8*	*35.3*	*41.4*	*72.6*	*315.1*	*70.7*	*300*	*600*	*bit*
356.80	*309.00*	*280Y1.20*	*7*	*7*	*6.5*	*25.0*	*53.6*	*67.3*	*333.8*	*74.6*	*300*	*600*	*bit*
357.68	309.76	281Y1.47	7	1	173.6	-12.8	263.3	-60.8	222.5	-84.9	300	600	"
358.49	310.46	282Y1.37	7	1	188.0	2.0	236.8	-53.1	197.7	-69.3	300	600	"
359.30	311.16	282Y2.41	7	3	177.8	13.0	253.5	-48.3	232.1	-71.3	300	600	"
360.64	312.32	283Y2.42	7	6	129.3	23.4	305.2	-22.6	315.8	-42.7	300	600	"
361.28	312.88	284Y1.11	7	5	172.4	10.0	261.8	-49.2	248.5	-74.0	300	600	"
362.25	313.72	284Y2.40	7	3	138.5	39.7	290.9	-20.2	297.2	-43.9	300	600	"
363.07	314.43	285Y1.53	7	6	132.9	-16.0	319.7	-39.3	343.1	-52.4	300	600	"
364.48	315.65	286Y2.20	7	10	240.4	54.0	204.5	-0.4	202.2	-10.2	300	600	"
365.38	316.43	287Y1.40	7	2	144.7	-2.2	302.1	-42.7	325.1	-62.2	300	600	"
366.87	317.72	288Y1.37	7	8	156.9	15.5	281.6	-41.8	291.1	-66.6	300	600	"
367.50	318.26	289Y1.23	7	5	165.3	9.2	272.4	-47.9	274.0	-73.5	300	600	"
368.24	318.91	289Y2.34	7	3	157.1	13.0	282.1	-43.1	292.7	-67.8	300	600	"
369.22	319.75	290Y1.43	6	6	162.9	4.2	277.1	-49.5	285.9	-74.8	300	575	"

mcd	msd	ID	n	MAD	bDec	bInc	bLon	bLat	rbLon	rbLat	T1	T2	Notes
369.94	320.38	290Y2.40	6	15	192.4	-4.7	228.1	-55.3	184.1	-67.1	300	575	"
370.78	321.10	291Y1.47	7	12	177.5	39.9	252.9	-32.2	243.0	-55.8	300	600	"
371.55	321.77	291Y2.51	7	5	166.2	25.8	267.7	-39.6	264.8	-65.1	300	600	"
372.44	322.54	292Y1.60	7	2	163.0	25.0	271.7	-39.2	272.2	-64.8	300	600	"
373.21	323.21	292Y2.61	7	2	181.3	11.7	248.2	-49.0	221.7	-70.3	300	600	PF7r
373.96	323.86	293Y1.60	7	2	15.5	3.8	43.3	53.8	2.3	64.0	300	600	PF8n
374.22	324.08	293Y2.10	7	5	21.3	22.2	25.6	59.5	339.5	60.2	300	600	PF8n
375.17	324.91	294Y1.28	7	3	174.1	-4.6	261.0	-56.8	233.4	-80.9	300	600	PF8r
375.96	325.59	294Y2.37	7	0	180.8	-12.2	248.6	-61.1	188.7	-79.2	300	600	"
376.61	*326.15*	*295Y1.51*	*7*	*22*	*37.0*	*55.9*	*326.6*	*60.1*	*304.3*	*41.3*	*300*	*600*	*MAD*
377.34	326.79	295Y2.53	7	1	188.7	10.5	237.0	-48.8	205.4	-66.0	300	600	"
378.15	327.49	296Y1.52	7	4	172.6	33.2	258.9	-36.3	250.6	-61.0	300	600	"
379.02	328.24	296Y2.64	7	3	165.6	6.2	272.7	-49.5	274.9	-75.1	300	600	"
379.49	328.65	297Y1.34	7	3	179.6	1.6	250.9	-54.1	216.8	-75.5	300	600	"
382.36	*331.13*	*299Y1.16*	*7*	*6*	*40.0*	*73.6*	*284.3*	*54.4*	*279.9*	*29.3*	*300*	*600*	*->R*
383.40	332.03	299Y2.43	7	6	167.4	17.4	267.8	-44.4	264.0	-69.9	300	600	PF8r
383.84	*332.42*	*300Y2.12*	*7*	*15*	*70.8*	*83.1*	*266.7*	*38.5*	*267.6*	*12.9*	*300*	*600*	*->R*
388.71	336.63	303Y1.41	7	6	25.8	22.0	19.1	56.8	339.2	55.8	300	600	PF9n
389.31	337.15	304Y2.34	7	2	351.9	22.7	89.7	65.6	298.6	88.7	300	600	"
391.94	339.43	305Y1.60	7	4	77.6	72.4	290.1	35.4	286.8	10.9	300	600	PF9n
392.66	340.05	305Y2.60	7	5	173.8	33.5	257.5	-36.3	248.3	-60.7	300	600	PF9r
393.07	340.41	306Y1.20	7	3	130.0	17.4	307.2	-25.5	319.5	-44.7	300	600	"
394.49	*341.64*	*307Y1.10*	*7*	*6*	*155.5*	*60.8*	*268.5*	*-9.9*	*267.9*	*-35.4*	*300*	*600*	*ovpr*
395.69	342.68	307Y2.71	7	7	358.8	33.6	74.2	73.3	298.3	79.3	300	600	
395.86	*342.82*	*308Y1.10*	*7*	*3*	*328.8*	*67.3*	*203.4*	*62.9*	*233.2*	*46.7*	*300*	*600*	*ovpr*
397.44	*344.19*	*309Y1.15*	*7*	*9*	*117.9*	*61.3*	*291.2*	*6.0*	*292.2*	*-18.0*	*300*	*600*	*ovpr*
398.80	345.37	310Y1.05	7	1	217.8	39.1	212.3	-22.5	199.7	-33.4	300	600	PF9r
399.78	346.22	310Y2.64	7	10	69.0	2.6	351.6	17.8	344.8	12.0	300	600	
400.18	346.57	310Y3.30	7	2	174.9	6.3	258.4	-51.5	237.9	-75.4	300	600	"
400.88	347.17	311Y1.54	7	2	144.9	7.0	298.0	-39.3	316.2	-60.4	300	600	PF9r
401.70	347.88	311Y2.70	7	3	323.6	11.0	127.3	45.3	154.9	62.5	300	600	PF10n
402.13	348.25	313Y1.27	7	16	330.9	18.3	123.2	53.1	161.4	70.2	300	600	"
402.99	349.00	313Y2.46	7	12	115.1	49.0	301.9	-0.8	304.8	-22.6	300	600	
404.20	350.05	314Y2.12	7	1	19.6	-7.7	40.9	46.9	9.6	57.9	300	600	"
404.99	350.73	315Y1.08	7	2	343.3	5.5	99.5	54.1	117.4	78.9	300	600	"
406.89	352.38	316Y1.61	7	3	342.8	48.8	144.7	74.5	233.1	69.7	300	600	"
407.49	352.90	317Y1.60	7	4	2.2	5.2	66.1	57.5	19.4	76.1	300	600	"
408.31	353.61	317Y2.66	7	5	27.1	7.9	25.2	50.0	351.9	53.5	300	600	"
408.97	354.18	318Y1.56	7	4	316.9	5.2	131.0	38.5	152.6	55.2	300	600	"
409.39	354.54	318Y2.27	7	9	353.2	33.2	91.5	72.0	270.4	82.4	300	600	"
410.14	*355.19*	*319Y1.20*	*7*	*39*	*15.6*	*19.3*	*37.0*	*61.1*	*343.7*	*65.7*	*300*	*600*	*MAD*

mcd is meters core depth and msd is meters stratigraphic depth of samples (ID) taken in core PFNP-1A, located at 35.09°N 250.20°E, that was deviated by 60° from horizontal toward azimuth of 135° in flat-lying strata. n is number of demagnetization steps between temperatures T1 and T2 (°C) used to calculate best-fit magnetization vector described by its maximum angular deviation (MAD; *Kirschvink*, 1980), the declination (bDec) and inclination (bInc) in bedding coordinates whose virtual geomagnetic pole is located at longitude (bLon) and latitude (bLat) with respect to present-day coordinates and rotated longitude (rbLon) and latitude (rbLat) with respect to a mean Late Triassic paleomagnetic reference pole for North America as was used in our previous study of the upper Chinle in PFNP-1A (210 Ma: 64.2°N 91.2°E [*Kent and Irving*, 2010]). Data in italicized red font were rejected for magnetostratigraphic interpretation of polarity because MAD>16°, data in italicized blue font had bInc>60° and were rejected as overprinted (ovpr), and samples with valid data are designated with constituent magnetozone in Notes.

Table S2. Paleomagnetic polarity intervals in core PFNP-1A.

Magneto-zone	Base, mcd	Base, msd	±, msd	Chron	Age, Ma	Ecc$_{405}$: k
PF1r	*47.40*	*41.05*	*0.41*	*E17r*	*209.49*	*517.73*
PF2n	*55.40*	*47.98*	*0.44*	*E17n*	*209.95*	*518.87*
PF2r	*74.49*	*64.51*	*2.70*	*E16r*	*210.25*	*519.60*
PF3n	*144.80*	*125.40*	*1.65*	*E16n*	*212.05*	*524.05*
PF3r.1r	*166.80*	*144.45*	*0.55*	*E15r.2r*	*212.36*	*524.82*
PF3r.1n	*172.60*	*149.48*	*1.63*	*E15r.1n*	*212.40*	*524.90*
PF3r	*177.67*	*153.87*	*0.48*	*E15r*	*212.60*	*525.41*
PF4n	*216.23*	*187.26*	*5.16*	*E15n*	*213.44*	*527.47*
PF4r	*249.10*	*215.73*	*1.77*	*E14r*	*214.92*	*531.15*
PF5n	310.61	268.99	0.54	E14n	216.16	534.19
PF5r	328.02	284.07	0.86	E13r	216.97	536.20
				E13n.2n	217.89	538.48
				E13n.1r	217.93	538.57
PF6n	340.30	294.70	0.55	E13n.1n	218.46	539.87
PF6r	345.94	299.58	0.31	E12r	219.29	541.93
PF7n	348.70	301.97	0.35	E12n	219.46	542.35
PF7r	374.34	324.18	0.33	E11r	221.47	547.31
PF8n	374.70	324.49	0.42	E11n	221.75	547.99
PF8r	386.06	334.33	2.30	E10r	222.24	549.22
PF9n	390.99	338.60	1.45	E10n	222.74	550.43
PF9r	401.29	347.52	0.36	E9r	224.01	553.57
PF10n	410.43	355.43		E9n	224.54	554.88

Magnetozone is the magnetic polarity interval numbered down from the uppermost identifiable polarity interval of the Chinle Fm. in this core (PF1r) to the lowermost polarity interval (PF10n) with a prefix, PF, for Petrified Forest and suffixes n and r for normal and reverse polarity. Italicized entries (PF1r to PF4r) are from Table S2 in [*Kent et al.*, 2018]. The identified base of each magnetozone is designated in mcd, meters core depth, and in msd, meters stratigraphic depth, msd, by taking into account the intended 60° inclination of the core hole; sampling resolution for polarity boundaries are given as ± msd. Correlative Chron for each magnetozone is given with its starting Age in million years ago (Ma) and position within a 405 kyr orbital eccentricity cycle (Ecc$_{405}$:k) where k is the fractional number of predicted cycles counting back from the most recent peak value (k=1) at 0.216 Ma [*Kent et al.*, 2017]. Reliable data for PF1r start in samples only at 38 mcd (~33 msd) above which the results are scattered due to weathering and drilling disturbance in the porous poorly lithified sediment; the base of PF10n corresponds to the unconformity between Chinle and underlying Moenkopi formations.

Table S3. Lithostratigraphic subdivisions of Chinle
Formation in core PFNP-1A compared to their relative
position in a composite outcrop section in and in the
vicinity of Petrified Forest National Park.

Rock units[&]	PFNP-1A, msd[#]	Composite height, m*
top (eroded) of Chinle Fm.	20.6	
base Owl Rock Mb.	41.7	290.0
base Black Forest Bed	66.9	262.0
base Petrified Forest Mb.	160.3	164.0
base Sonsela Mb.	278.9	78.0
base Blue Mesa Mb.	331.2	30.0
base Mesa Redonda Mb. (=base Chinle Fm.)	355.4	0.0

[&]*Martz and Parker* [2010]. [#]Meters stratigraphic depth for a core
hole inclination of 60° in flat-lying strata [*Olsen et al.*, 2018].
*composite outcrop section [*Atchley et al.*, 2013]. Linear
regression: Y= 358.9 – 1.115X, where Y is msd in PFNP-1A and
X is height in outcrop in meters.

Table S4. High precision U-Pb CA-TIMS detrital zircon ages reported for Chinle Formation in PFNP and vicinity.

ID		Unit	Level		Age	±2σ	Ref.
			mcd	msd	Ma	Myr	
Core PFNP-1A samples							
52Q2	(N)	BFB	64.6	56.0*	210.08	0.22	1
158Q2	(N)	Sonsela	198.6	172.0	213.55	0.28	1
177Q1	*(N)*	*Sonsela*	*219.4*	*190.0*	*212.81*	*1.25*	*1*
182Q1	(N)	Sonsela	225.5	195.3	214.08	0.20	1
Outcrop samples projected to core PFNP-1A							
BFB	(N)	BFB		66.7*	209.93	0.26	2
GPU	(S)	Sonsela		186.0	213.12	0.27	2
KWI	(N)	Sonsela		188.2	213.87	0.27	2
P57-C	(N)	Sonsela		194.9	213.63	0.28	3
GPL	(S)	Sonsela		222.8	218.02	0.28	2
SBJ	(S)	Sonsela		243.3	219.32	0.27	2
SS-7	(S)	Blue Mesa		278.6	220.12	0.07	4
TPs	(S)	Blue Mesa		287.5	223.04	0.27	2
SS-28	(HV)	Mesa Redondo		333.3	225.18	0.28	2
SS-24	(HV)	Mesa Redondo		356.6	227.60	0.08	4

ID are samples with locations (N for northern PFNP, S for southern PFNP, HV for Hunt Valley; **Fig. 1C**) taken from various lithostratigraphic units in the Chinle Formation (BFB is Black Forest Bed within the Petrified Forest Member) at levels in PFNP-1A corresponding to meters core depth (mcd) and meters stratigraphic depth (msd) by accounting for 60° core hole inclination and assuming flat lying strata. Sample 177Q1 had an anomalously young age presumably due to residual Pb-loss and was not used in age models. The equivalent msd for each outcrop sample was projected to core PFNP-1A by correlation of the lithostratigraphy of the measured cumulative section [*Atchley et al.*, 2013; *Ramezani et al.*, 2011]; see **Table S3** for stratigraphic levels used in linear regression shown in **Figure 4**. There may be differences on the order of 10 m and sometimes more with the registry of individual outcrop samples with other schemes (e.g., *Martz and Parker*, 2010]. *The apparent difference in stratigraphic levels for BFB may simply reflect that core sample 52Q2 was taken higher in the thick tuffaceous sandstone unit than at the base as for BFB sample in outcrop. Ref.: 1, *Kent et al.* [2018]; 2, *Ramezani et al.* [2011]; 3, *Nordt et al.* [2015]; 4, *Atchley et al.* [2013].